IMPLEMENTING MULTI-SCALE AGRICULTURAL INDICATORS EXPLOITING SENTINELS

VEGETATION FIELD DATA AND PRODUCTION OF GROUND-BASED MAPS:

"COLLELONGO SITE - SELVAPIANA, ITALY" 8TH JULY AND 25TH SEPTEMBER, 2015

ISSUE I1.10

EC Proposal Reference N° FP7-311766

Actual submission date : March 2016

Start date of project: 01.11.2012 Duration : 40 months

Name of lead partner for this deliverable: EOLAB

Book Captain: Consuelo Latorre (EOLAB)

Contributing Authors: Fernando Camacho, María del Carmen Piñó (EOLAB)
Enrica Nestola, Carlo Calfapietra, Giorgio Matteucci (IBAF-CNR)

Project co-funded by the European Commission within the Seventh Framework Program (2007-2013)		
Dissemination Level		
PU	Public	**X**
PP	Restricted to other programme participants (including the Commission Services)	
RE	Restricted to a group specified by the consortium (including the Commission Services)	
CO	Confidential, only for members of the consortium (including the Commission Services)	

DOCUMENT RELEASE SHEET

Book Captain:	C. Latorre	Date: 30.01.2017	Sign. 
Approval:	R. Lacaze	Date: 08.02.2017	Sign. 
Endorsement:	I. Simion	Date:	Sign.
Distribution:	Public		

CHANGE RECORD

Issue/Revision	Date	Page(s)	Description of Change	Release
	11.03.2016	All	First Issue	I1.00
I1.00	30.01.2017	All	Correction ground values	I1.10

TABLE OF CONTENTS

LIST OF FIGURES

LIST OF TABLES

LIST OF ACRONYMS

CEOS	Committee on Earth Observation Satellite
CEOS LPV	Land Product Validation Subgroup
CNR	National Research Council (Italy)
CONECOFOR	*CONtrolli ECOsistemi FORestali*
DG AGRI	Directorate General for Agriculture and Rural Development
DG RELEX	Directorate General for External Relations (European Commission)
DHP	Digital Hemispheric Photographs
ECV	Essential Climate Variables
EUROSTATS	Directorate General of the European Commission
ESU	Elementary Sampling Unit
EUNIS	European Nature Information System
FAPAR	Fraction of Absorbed Photo-synthetically Active Radiation
FAO	Food and Agriculture Organization
FCOVER	Fraction of Vegetation Cover
FLUXNET	Fluxes Network of regional networks
GCOS	Global Climate Observing System
GEO-GLAM	Global Agricultural Geo- Monitoring Initiative
GIO-GL	GMES Initial Operations - Global Land (GMES)
GCOS	Global Climate Observing System
GMES	Global Monitoring for Environment and Security
GPS	Global Positioning System
IBAF	Institute of Agro-Environmental & Forest Biology (Italy)
ICP-Forest	International Co-operative Program on assessment and monitoring of air pollution effects on forest
IMAGINES	Implementing Multi-scale Agricultural Indicators Exploiting Sentinels
JECAM	Joint Experiment for Crop Assessment and Monitoring
LAI	Leaf Area Index
LDAS	Land Data Assimilation System
LIFE+	*L'instrument Financiaire pour L'Enviroment*
LTER	Long-Term Ecosystem Research
LUT	Look-up-table techniques
PAI	Plant Area Index
PASTIS–PAR	PAI Autonomous System from Transmittance Sensors.
PRIN	*Progetto di Rilevante Interesse Nazionale*
PROBA-V	Project for On-Board Autonomy satellite, the V standing for vegetation.
RMSE	Root Mean Square Error

SPOT /VGT	Satellite Pour l'Observation de la Terre / VEGETATION
SCI	GMES Services Coordinated Interface
SLT	Solar Local Time
TOC	Top of Canopy Reflectance
USGS	U.S. Geological Survey Science organization
UTM	Universal Transverse Mercator coordinates system
VALERI	Validation of Land European Remote sensing Instruments
WGCV	Working Group on Calibration and Validation (CEOS)

1. BACKGROUND OF THE DOCUMENT

1.1. EXECUTIVE SUMMARY

The Copernicus Land Service has been built in the framework of the FP7 geoland2 project, which has set up pre-operational infrastructures. ImagineS intends to ensure the continuity of the innovation and development activities of geoland2 to support the operations of the global land component of the GMES Initial Operation (GIO) phase. In particular, the use of the future Sentinel data in an operational context will be prepared. Moreover, IMAGINES will favor the emergence of new downstream activities dedicated to the monitoring of crop and fodder production.

The main objectives of ImagineS are to (i) improve the retrieval of basic biophysical variables, mainly LAI, FAPAR and the surface albedo, identified as Terrestrial Essential Climate Variables, by merging the information coming from different sensors (PROBA-V and Landsat-8) in view to prepare the use of Sentinel missions data; (ii) develop qualified software able to process multi-sensor data at the global scale on a fully automatic basis; (iii) complement and contribute to the existing or future agricultural services by providing new data streams relying upon an original method to assess the above-ground biomass, based on the assimilation of satellite products in a Land Data Assimilation System (LDAS) in order to monitor the crop/fodder biomass production together with the carbon and water fluxes;(iv) demonstrate the added value of this contribution for a community of users acting at global, European, national, and regional scales.

Further, ImagineS serves the growing needs of international (e.g. FAO and NGOs), European (e.g. DG AGRI, EUROSTATS, DG RELEX), and national users (e.g. national services in agro-meteorology, ministries, group of producers, traders) on accurate and reliable information for the implementation of the EU Common Agricultural Policy, of the food security policy, for early warning systems, and trading issues. ImagineS will also contribute to the Global Agricultural Geo-Monitoring Initiative (GEO-GLAM) by its original agriculture service which can monitor crop and fodder production together with the carbon and water fluxes and can provide drought indicators, and through links with JECAM (Joint Experiment for Crop Assessment and Monitoring).

1.2. PORTFOLIO

The ImagineS portfolio contains global and regional biophysical variables derived from multi-sensor satellite data, at different spatial resolutions, together with agricultural indicators, including the above-ground biomass, the carbon and water fluxes, and drought indices resulting from the assimilation of the biophysical variables in the Land Data Assimilation System (LDAS).

The production in Near Real Time of the 333m resolution products, at a frequency of 10 days, using PROBA-V data is carried out in the Copernicus Global Land Service (http://land.copernicus.eu/global/).

The demonstration of high resolution (30m) products derived from Landsat-8 was done over demonstration sites of cropland and grassland in contrasting climatic and environmental

conditions. Demonstration products are available on the ImagineS website (http://www.fp7-imagines.eu/pages/services-and-products/landsat-8-biophysical-products.php)

1.3. SCOPE AND OBJECTIVES

The main objective of this document is to describe the field campaign and ground data collected at Collelongo-Selvapiana experimental site in Collelongo (AQ) Italy, and the up-scaling of the ground data to produce ground-based high resolution maps of the following biophysical variables:

- Leaf Area Index (LAI), defined as half of the total developed area of leaves per unit ground surface area (m^2/m^2). We focused on two different LAI quantities (for green elements):
  - The effective LAI (LAIeff) derived from the description of the gap fraction as a function of the view zenith angle. In addition, effective LAI measures derived at 57.5º are also provided in the ground database.
  - The actual LAI (LAI) corrected from the clumping index.
- Fraction of green vegetation cover (FCover), defined as the proportion of soil covered by vegetation, derived from the gap fraction between 0 and 10º of view zenith angle.
- Fraction of Absorbed Photosynthetically Active Radiation (FAPAR), which is the fraction of the photosynthetically active radiation (PAR) absorbed by a vegetation canopy. We are also focused on green elements. PAR is the solar radiation reaching the canopy in the 0.4–0.7 µm wavelength region. We focused on the instantaneous 'black-sky' FAPAR at 10:00h Solar Local Time (SLT), which is the FAPAR under direct illumination conditions at a given solar position. In addition, two other quantities are provided: daily integrated FAPAR computed as the black-sky FAPAR integrated over the day and the 'white-sky' FAPAR, which is the FAPAR under diffuse illumination conditions.

1.4. CONTENT OF THE DOCUMENT

This document is structured as follows:

- Chapter 2 provides an introduction to the field experiment.
- Chapter 3 provides the location and description of the site.
- Chapter 4 describes the ground measurements, including material and methods, sampling and data processing.
- Chapter 5 provides an evaluation of the sampling.
- Chapter 6 describes the production of high resolution ground-based maps, and the selected "mean" values for validation.

2. INTRODUCTION

Validation of remote sensing products is mandatory to guaranty that the satellite products meets the user's requirements. Protocols for validation of global LAIeff products are already developed in the context of Land Product Validation (LPV) group of the Committee on Earth Observation Satellite (CEOS) for the validation of satellite-derived land products (Fernandes *et al.,* 2014), and recently applied to Copernicus global land products based on SPOT/VGT observations (Camacho *et al*., 2013). This generic approach is made of 2 major components:

- The indirect validation: including inter-comparison between products as well as evaluation of their temporal and spatial consistency

- The direct validation: comparing satellite products to ground measurements of the corresponding biophysical variables. In the case of low and medium resolution sensors, the main difficulty relies on scaling local ground measurements to the extent corresponding to pixels size. However, the direct validation is limited by the small number of sites, for that reason a main objective of ImagineS is the collection of ground truth data in demonstration sites.

The content of this document is compliant with existing validation guidelines (for direct validation) as proposed by the CEOS LPV group (Morisette et al., 2006); the VALERI project (http://w3.avignon.inra.fr/valeri/) and ESA campaigns (Baret and Fernandes, 2012). It therefore follows the general strategy based on a bottom up approach: it starts from the scale of the individual measurements that are aggregated over an elementary sampling unit (ESU) corresponding to a support area consistent with that of the high resolution imagery used for the up-scaling of ground data. Several ESUs are sampled over the site. Radiometric values over a decametric image are also extracted over the ESUs. This will be later used to develop empirical transfer functions for up-scaling the ESU ground measurements (e.g. Martínez et al., 2009). Finally, the high resolution ground based map will be compared with the medium resolution satellite product at the spatial support of the product.

In the framework of ImagineS project, a multi-temporal field experiment to characterize the vegetation biophysical parameters at the Collelongo site, a beech forest in Italy, was carried out by EOLAB and IBAF (Institute of Agro-Environmental & Forest Biology of the National Research Council - CNR). Moreover, in early May 2015, IBAF installed the PASTIS-PAR system developed by INRA-Hiphen to continuous monitoring PAR over different points in 1 km area around the flux tower of the experimental site.

During 2015, two main activities were conducted: (1) Two field campaigns on 8th July and 25th September, 2015 for the spatial characterization of vegetation variables in the study area, conducted by EOLAB (8th July) and IBAF (25th September), and (2) set-up of PASTIS-PAR (PAI Autonomous System from Transmittance Sensors) systems for the continuous monitoring of FAPAR and Plant Area Index (PAI). The PASTIS-PAR sensors were installed from May to December.

This report describes the field activities during the two campaigns carried out in 2015, as well as the ground data processing and up-scaling with Landsat-8 imagery. The PASTIS-PAR data will be reported separately at the end of the project.

Field Campaigns:

- **First campaign: 8th of July, 2015**
- **Second campaign: 25th of September, 2015**

Figure 1: Team involved in the field campaign in Collelongo site, Italy (2015). Left: Fluxnet Tower, operators Consuelo Latorre and Giorgio Matteucci. Right: Operators Enrica Nestola and Fernando Camacho.

Contact:

EOLAB: Fernando Camacho (fernando.camacho@eolab.es)

IBAF-CNR: Enrica Nestola (enrica.nestola@ibaf.cnr.it)

Teams involved in field collection (Figure 1):

IBAF – CNR: G. Matteucci, E. Nestola

EOLAB: F. Camacho, C. Latorre

3. STUDY AREA

3.1. LOCATION

The study area is located in Selvapiana, at the beech forest in Collelongo (Italy), managed by IBAF - CNR (Figure 2). Collelongo-Selva Piana beech forest (Abruzzo region, Central Italy, 41°50′58″N, 13°35′17″E, 1500 m elevation) is part of a wider forest area, included in the external belt of the Abruzzo National Park (Table 3). The Selva Piana stand is located within a 3000 ha community forest and its structure and conditions are representative of Central Apennine beech forests.

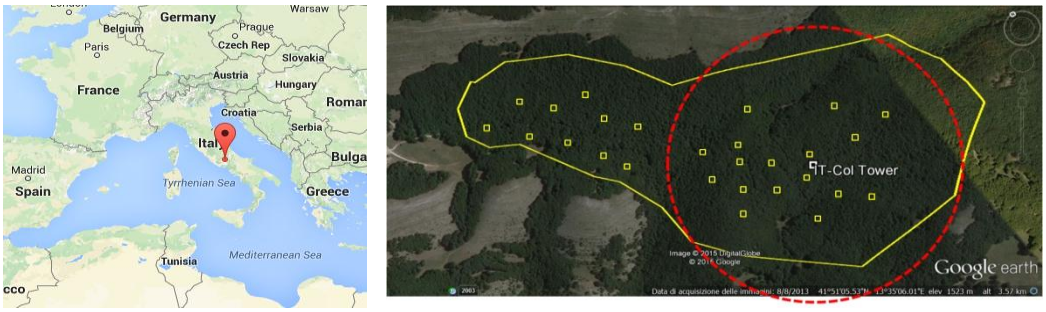

Location Study area from GoogleEarth

Figure 2: Location of Collelongo-Selvapiana experimental site in Collelongo, Italy.

Table 1: Coordinates and altitude of the test site (centre).

CAMPAIGN	Altitude	Latitud	Longitude
Collelongo Geographic Lat/Lon, WGS 84 (degrees)	1500m	41.85º N	13.59º E

Figure 3 shows the false color composition of the test site (5x5 km^2) using Landsat-8 Top Of Canopy (TOC) Reflectance SWIR-NIR-RED channels. Landsat-8 TOC reflectance data was used for up-scaling.

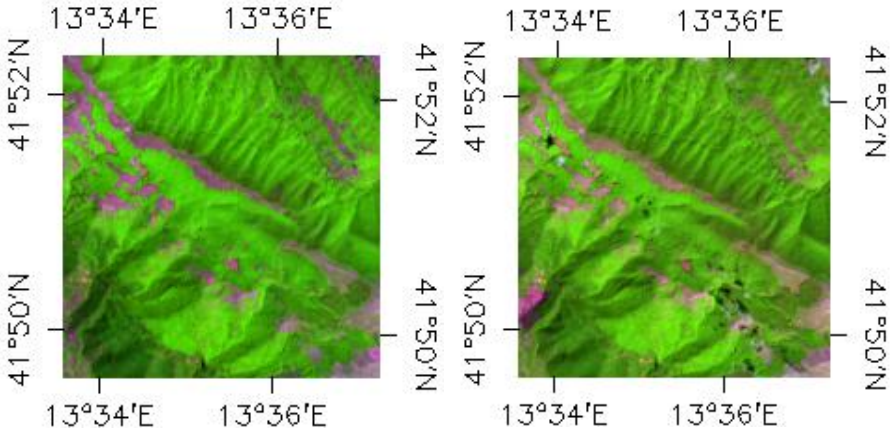

Figure 3: False color composition (SWIR-NIR-RED) of TOC Reflectance Landsat-8 images over the Collelongo study area 5x5 km^2. Left side: 8th July 2015. Right side: 25th September 2015.

3.2. DESCRIPTION OF THE TEST SITE

The permanent experimental site was installed in 1991 by the Department of Forest Environment and Resources, University of Tuscia, Viterbo, Italy and take part in several international networks as CarboEurope, FluxNet or ICP-Forests.

The climate is Mediterranean montane, with cool summer and long cold winters and a mean annual temperature of 7.1 °C. Mean annual precipitation for the period 1996 – 2007 is 1104 mm year^{-1}, of which ~10% falls in summer. According to EUNIS (European Nature Information System) habitat classification, the site is included into the Southern Italian beech forests type. Vegetation is homogeneous and dominated by European beech (Fagus sylvatica L.); soil has a variable depth ranging from 40 to 100 cm and is classified as humic soil (Chiti et al., 2010).

In the area of the experimental site, the density is 830 trees ha^{-1}, the average basal area is 39.4 m^2 ha^{-1} with a mean diameter at breast height of 24.6 cm (sampling trees with diameter >1 cm) and a mean height of 21.2 m (data from the 2002 survey). Over a period of 10 years, stand leaf area index (LAI) ranged between 4.5 and 6.5. A detailed description of the site and of the stand structure has been reported in other works (Guidolotti et al., 2013; Scartazza et al., 2013; Matteucci et al., 2007). The site is equipped with an eddy-covariance tower measuring the exchange of CO_2, H_2O and energy fluxes since 1993 (Valentini et al. 1996). Collelongo-Selvapiana experimental site is currently part of the following projects: LIFE+ Smart4Action, LTER H2020, PRIN 2012 Nitrogen in Mediterranean Forest, CNR IBAF Ecology and Dynamics of Forest Systems. It is also part of international networks as LTER-Europe, Fluxnet, ICP-Forests, ICP-Integrated Monitoring and CONECOFOR programs.

Figure 4 shows some pictures taken under and above the canopy from the flux tower.

Figure 4: Pictures taken during the field campaigns (2015) in *Collelongo site* (Italy).

4. GROUND MEASUREMENTS

The ground measurement database reported here was acquired by EOLAB (first campaign) and IBAF (second campaign).

4.1. MATERIAL AND METHODS

4.1.1 Digital Hemispheric Photographs (DHP)

DHP were acquired with a digital camera. Hemispherical photos allow the calculation of LAI, FAPAR and FCOVER measuring gap fraction through an extreme wide-angle camera lens (i.e. 180º) (Weiss et al., 2004). It produces circular images that record the size, shape, and location of gaps, either looking upward from within a canopy or looking downward from above the canopy. Two hemispherical digital photography (DHP) cameras were used for estimating biophysical variables in the study area: CANON EOS 6D with a SIGMA 8mm F3.5 – EX DG and NIKON Coolpix 995-FCE8.

Since optical systems are not perfect, it is needed to calibrate the system in order to determinate the Optical Centre and the Projection Function (Weiss, 2010). The optical centre is defined by the projection of the optical axis onto the CCD matrix where the image is recorded, for the CANON EOS 6D dual system (camera and lens) was found in the point: (x=1378, y=896) (Latorre et al. 2014). For the NIKON camera the point was: (x=851, y=998).

The hemispherical photos acquired during the field campaign were processed with the CAN-EYE software version 6.4 (developed by INRA http://www6.paca.inra.fr/can-eye) to derive LAI, FAPAR and FCOVER. It is based on a RGB colour classification of the image to discriminate vegetation elements from background (i.e., gaps). This approach allows exploiting downward-looking photographs for short canopies (background = soil) as well as upward-looking photographs for tall canopies (background = sky). CAN-EYE software processes simultaneously up to of 20 images acquired over the same ESU. Note that our images were acquired with similar illumination conditions to limit the variation of colour dynamics between images.

The processing is achieved in 3 main steps (Weiss et al., 2004). First, image pre-processing is performed, which includes removing undesired objects (e.g. operator, sun glint) and image contrast adjustments to ensure a better visual discrimination between vegetation elements and background. Second, an automatic classification (k-means clustering) is applied to reduce the total number of distinctive colours of the image to 324 which is sufficient to ensure accurate discrimination capacities while keeping a small enough number of colours to be easily manipulated. Finally, a default classification based on predefined colour segmentation is first proposed and then iteratively refined by the user. The allocation of the colours to each class (vegetation elements versus background) is the most critical phase that needs to be interactive because colours depend both on illumination conditions and on canopy elements. At the end of this process a binary image, background versus vegetation elements (including both green and non-green elements) is obtained.

The CAN-EYE software computes biophysical variables from gap fraction as follows:

Effective LAI (LAIeff): Among the several methods described in Weiss et al (2004), the effective LAI estimation in the CAN-EYE software is performed by model inversion. The effective LAI is estimated from the Plant Area Index (PAI) which is the variable estimated by CAN-EYE, as no distinction between leaves or other plant elements are made from the gap fraction estimates. PAI is very close to the effective LAI for croplands when pictures are taken downward looking, whereas larger discrepancies are expected for forest when pictures are taken upward looking. Effective LAI is directly retrieved by inverting Eq. (1) (Poisson model) and assuming an ellipsoidal distribution of the leaf inclination using look-up-table (LUT) techniques.

$$P_0(\theta_v, \varphi_v) = e^{-N\cdot(\theta_v,\varphi_v)} = e^{-G\cdot(\theta_v,\varphi_v)\cdot\frac{LAI_{eff}}{\cos(\theta_v)}} \quad \text{Eq. (1)}$$

A large range of random combinations of LAI (between 0 and 10, step of 0.01) and ALA (Average Leaf Angle) (10º and 80º, step of 2º) values is used to build a database made of the corresponding gap fraction values (Eq.1) in the zenithal directions defined by the CAN-EYE user (60º for the DHP collection in this field campaign). The process consists then in selecting the LUT element in the database that is the closest to the measured P_0. The distance (cost function C_k) of the k^{th} element of the LUT to the measured gap fraction is computed as the sum of two terms. The first term computes a weighted relative root mean square error between the measured gap fraction and the LUT one. The second term is the regularization term that imposes constraints to improve the PAI estimates. Two equations are proposed for the second “regularization” term:

(1) constraint used in CAN-EYE V5.1 on the retrieved ALA values that assume an average leaf angle close to 60º ± 03º, and

(2) constraint used in CAN-EYE V6.1 on the retrieved PAI value that must be close from the one retrieved from the zenithal ring at 57º. This constraint is more efficient, but it can be computed only when the 57º ring is available (i.e., COI≥60º)

The software also proposed other ways of computing PAI and ALA effective using Miller’s formula (Miller, 1967) which assumed that gap fraction only depends from view zenith angle. Furthermore, the CAN-EYE makes an estimation using the Welles and Norman (1991) method used in LAI-2000 for 5 rings. These LAI2000-like estimates were not used here as are based on the same Miller’s formula but using limited angular sampling.

LAI: The actual LAI that can be measured only with a planimeter with however possible allometric relationships to reduce the sampling, is related to the effective leaf area index through:

$$LAI_{eff} = \lambda_0 \cdot LAI \quad \text{Eq. (2)}$$

where λ_0 is the clumping index. In CAN-EYE, the clumping index is computed using the Lang and Xiang (1986) logarithm gap fraction averaging method, although some uncertainties are associated to this method (Demarez et al., 2008). The principle is based on the assumption that vegetation elements are locally assumed randomly distributed. Values of clumping index given by CAN_EYE are in certain cases correlated with the size of the cells used to divide photographs. The values reported here were estimated with an average of the three results (CEV6.1, CEV5.1 and Miller).

As the CAN-EYE software provides different results (CEV6.1, CEV5.1 and Miller's) for LAIeff and LAI variables; an average LAI value was provided as ground estimate, and the standard deviation of the different method LAI estimates was reported as the uncertainty of the estimate (see associated ***2015_VGM_Collelongo.xls*** *file). Note that for LAI, only CEV6.1 and CEV5.1 were used.*

FCOVER is retrieved from gap fraction between 0 to 10°.

$$FCOVER = 1 - P_0 \cdot (0 - 10°) \quad \text{Eq. (3)}$$

The standard deviation calculated over different pictures is provided by the CAN-EYE software. The FCover along with the standard deviation (uncertainty) is provided in the field data file (2015_VGM_Collelongo.xls).

FAPAR**:** As there is little scattering by leaves in that particular spectral domain due to the strong absorbing features of the photosynthetic pigments, FAPAR is often assumed to be equal to FIPAR (Fraction of Intercepted Photosynthetically Active Radiation), and therefore directly related to the gap fraction. The actual FAPAR is the sum of two terms, weighted by the diffuse fraction in the PAR domain: the 'black sky' FAPAR that corresponds to the direct component and the 'white sky' or the diffuse component.

The instantaneous "Black-sky FAPAR" ($FPAR^{BS}$) is given at a solar position (date, hour and latitude). Depending on latitude, the CAN EYE software computes the solar zenith angle every solar hour during half the day (there is symmetry at 12:00). The instantaneous FAPAR is then approximated at each solar hour as 1 minus the gap fraction in the corresponding solar zenith angle:

$$FAPAR^{BS}(\theta_S) = 1 - P_0 \cdot (\theta_S) \quad \text{Eq. (4)}$$

The daily integrated "black-sky" FAPAR is computed as the following:

$$FAPAR^{BS}_{Day} = \frac{\int_{sunset}^{sunrise} cos(\theta_S) \cdot [1 - P_0 \cdot (\theta_S)] \cdot d\theta}{\int_{sunset}^{sunrise} cos(\theta_S) \cdot d\theta} \quad \text{Eq. (5)}$$

The "white-sky" (or diffuse) FAPAR is computed as the following:

$$FAPAR^{WS} = \frac{1}{\pi} \int_0^{2\cdot\pi} \int_0^{\frac{\pi}{2}} P_0 cos(\theta_S) sin(\theta_S) d\theta d\varphi = 2 \cdot \int_0^{\frac{\pi}{2}} P_0 cos(\theta_S) sin(\theta_S) d\theta \quad \text{Eq. (6)}$$

The CAN-EYE software provides the three FAPAR variables. Instantaneous black-sky FAPAR values at 10:00h SLT were up-scaled. No uncertainty is provided on the FAPAR estimates.

4.2. SPATIAL SAMPLING SCHEME

A pseudo-regular sampling was used within each Elementary Sampling Unit (ESU) of approximately 20x20 m^2. The centre of the ESU was geo-located using a Global Positioning System (GPS). A total of 15 ESUs were characterized each campaign (same locations) following the main access road (Figure 5). The number of hemispherical photos per ESU ranges between 12 and 15. In several ESUs, continuous measurements were taken with PASTIS-PAR devices for monitoring the seasonal cycle.

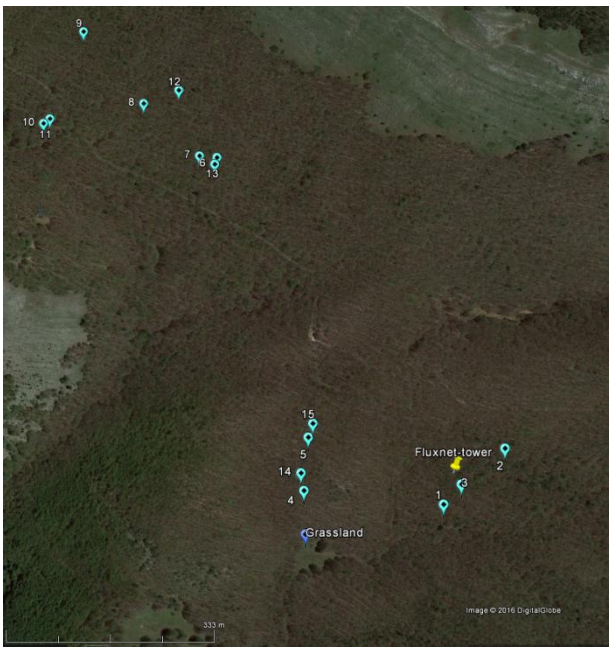

Figure 5: Distribution of the Elementary Sampling Units (ESU) over the study area in *Collelongo* site. ESU location over Google Earth.

The spatial sampling scheme was predefined to cover the variability of the site around the flux tower area. Additional elementary sampling units (ESU) were selected from the image to complete the representation of the variability in the study area, such as Bare Soil (BS) estimated by visual inspection.

Due the forest canopy homogeneity around the area of study, four bare soil were selected out of the 5x5 Km area centered on 41.85º N, 13.59º E for both campaigns on July and September, 2015, by a visual selection based on low NDVI values (table 2).

Table 2: Additional control points considered for bare soil based on NDVI values (July and September) and one additional grassland measurement (July).

Soil type	Latitude	Longitude	NDVI 2015-07-08	NDVI 2015-09-25
Bare soil	42.063777	13.407041	0.17	0.15
Bare soil	42.007504	13.631606	0.15	0.12
Bare soil	41.993379	13.819525	0.16	0.07
Bare soil	41.985572	13.519085	0.18	0.17
Grassland	41.848340	13.585495	0.76	-

For the campaign performed in July, and to increase the variability over the NDVI medium ranges to improve the transfer function results, an ESU categorized as "grass" was included (figure 5 -data field as blue and additional ESU as red- and table 3)

4.3. GROUND DATA

4.3.1. Data processing

The software CAN-EYE version V6.4 was used to process the DHP images. Figure 6 shows some examples of DHP over several ESUs.

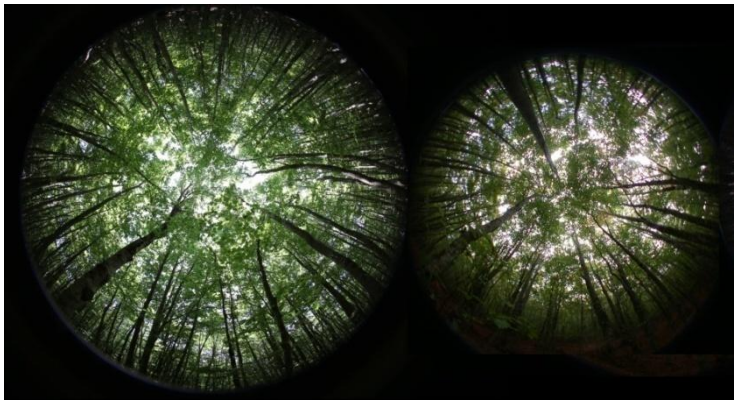

Figure 6: Digital Hemispherical Photographs acquired in Collelongo site (Italy) during the field campaigns in 2015, ESU 9. Left: First field campaign (8th July). Right: Second field campaign (25th September).

Figure 7 shows an example of the CAN-EYE processing results carried out on ESU 3 during the first field campaign (8th July, 2015). Different results of the CAN-EYE processing are selected, including the DHP (a), and the green/sky classification (b), the average gap fraction (c) and the clumping factor versus view zenith angle (d).

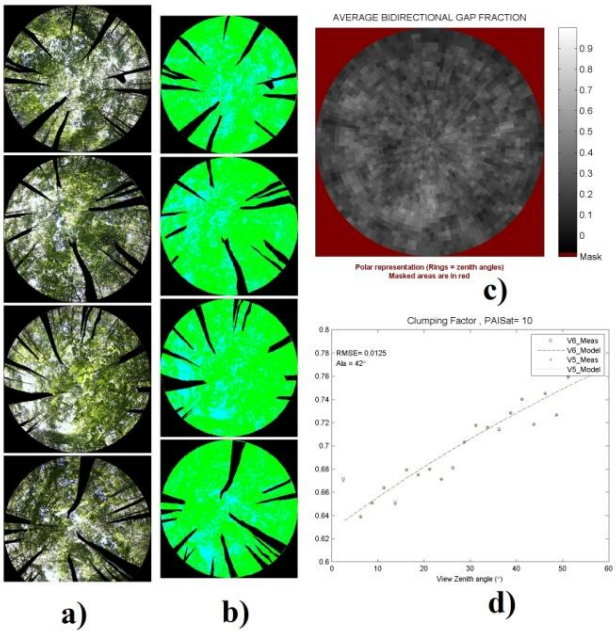

Figure 7: Results of the CAN-EYE processing carried out on ESU 3 during the first field campaign (8th July, 2015): (a) DHP images, (b) classified images, (c) average gap fraction and (d) the clumping factor versus view zenith angle.

As described in section 4.1, CAN-EYE provides the LAI and effective LAI values by using three different methods: CEV6.1, CEV5.1 and Miller's. Figure 8 show the results for the three methods versus the average value. For LAIeff, the results are very similar and the average of the three estimations is provided on the ground dataset. However, for the LAI, the scattering between methods is much higher, displaying Miller's method lowest estimations than CEV6.1 and CEV5.1. It can be partly explained due to the fact that Miller's method does not consider all the viewing angles for the clumping estimation. Thus, Miller's LAI retrievals have been discarded for computing the LAI averaged value provided in the ground dataset.

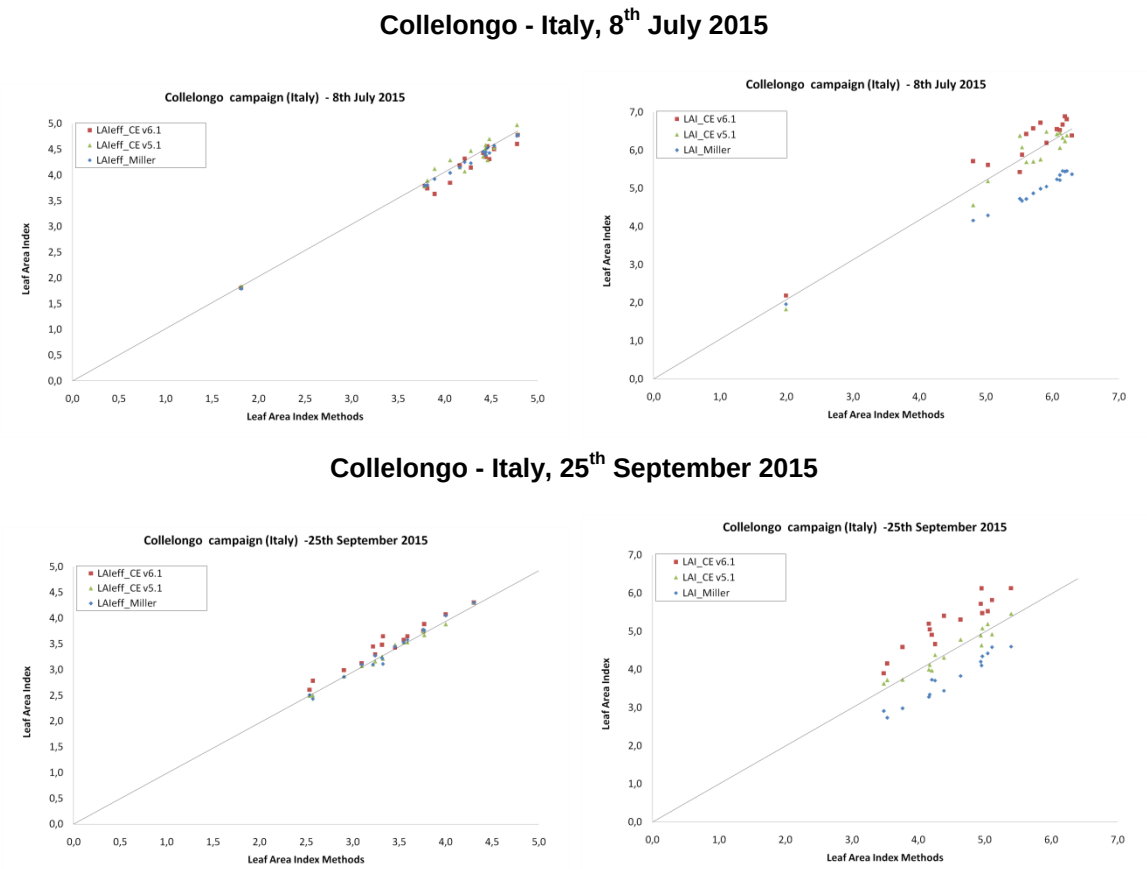

Figure 8: Inter-comparison of the estimated biophysical variables LAIeff (left side) and LAI (right side) over the ESUs with different methods: CEV5.1, CEV6.1 and Miller´s formula. Top: First campaign on 8th July, 2015. Bottom: Second campaing on 25th September 2015.

Figure 9 shows the relation between LAI with instantaneous FAPAR at 10:00 SLT. The typical positive exponential curve is observed. Both campaigns are presented at the same graph where similar values can observed, but slightly higher for the second one (green dots).

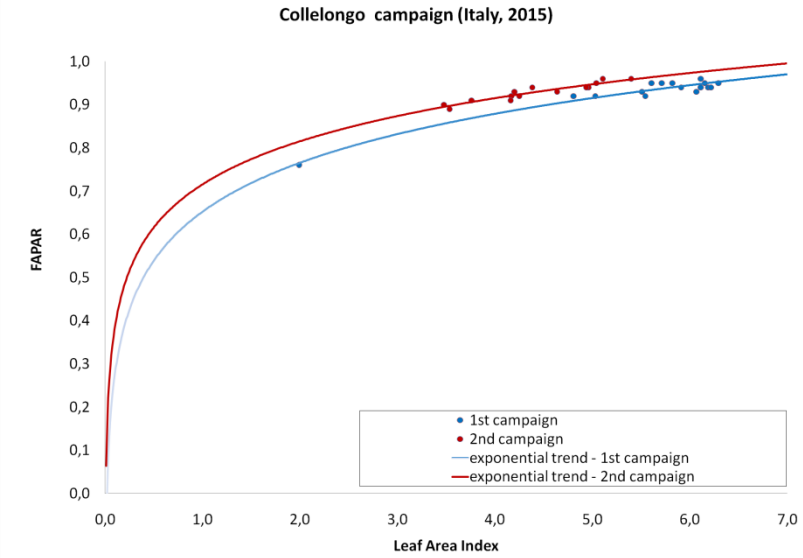

Figure 9: FAPAR vs LAI ground measurements at the Collelongo site (Italy). First campaign on 8th July (blue dots) and second campaign on 25th September (red dots).

Figure 10 shows the relationship between FAPAR and FCOVER values, the typical linear trend between both variables is observed, with slightly higher values for the FAPAR as expected.

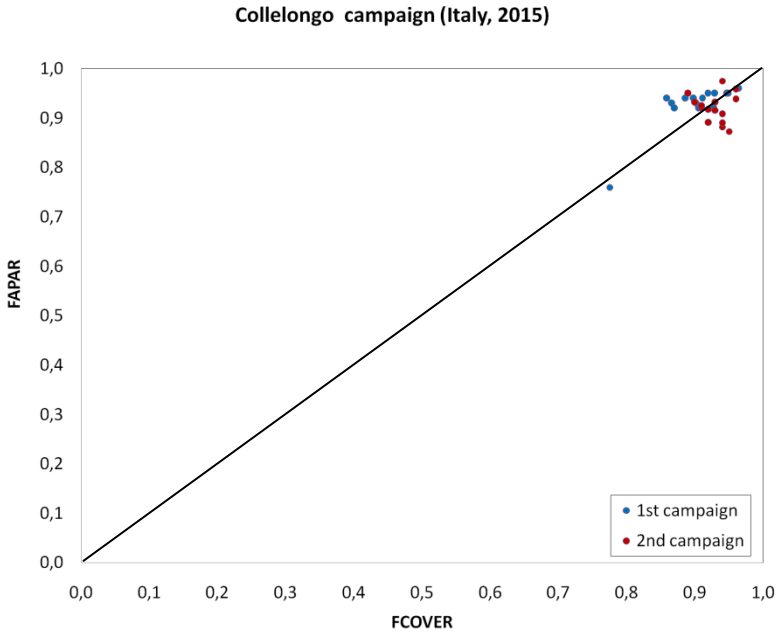

Figure 10: FAPAR versus FCOVER ground measurements at the Collelongo site (Italy). Left side: First field campaign (8th July) (blue dots). Right side: Second field campaign (25th September) (red dots).

4.3.2. Content of the Ground Dataset

Each ESU is described according to a standard format. The header of the database is shown in Table 3. The ground data is provided in the associated field "2015_VGM_Collelongo.xlsx"

Table 3: The Header used to describe ESUs with the ground measurements.

Column	Var.Name		Comment
1	Plot #		Number of the field plot in the site
2	Plot Label		Label of the plot in the site
3	ESU #		Number of the Elementary Sampling Unit (ESU)
4	ESU Label		Label of the ESU in the campaign
5	Northing Coord.		Geographical coordinate: Latitude (º), WGS-84
6	Easting Coord.		Geographical coordinate: Longitude (º), WGS-84
7	Extent (m) of ESU (diameter)		Size of the ESU [(1)]
8	Land Cover		Detailed land cover
9	Start Date (dd/mm/yyyy)		Starting date of measurements
10	End Date (dd/mm/yyyy)		Ending date of measurements
11	Products*	Method	Instrument
12		Nb. Replications	Number of Replications
13		PRODUCT	Methodology
14		Uncertainty	Standard deviation

*LAIeff, LAI, FAPAR and FCOVER

Figure 11 shows the measurements obtained during the two field experiments.

The LAIeff ranges between 1.86 and 3.14 for the first campaign and between 2.33 and 3.14 for the second one. Similar distributions were obtained for LAI, with higher values due to the correction of the clumping. Averaged values for LAI are 3.62 for the first campaign and 3.78 for the second campaign, which indicates a quite stable status of the canopy during the summer period.

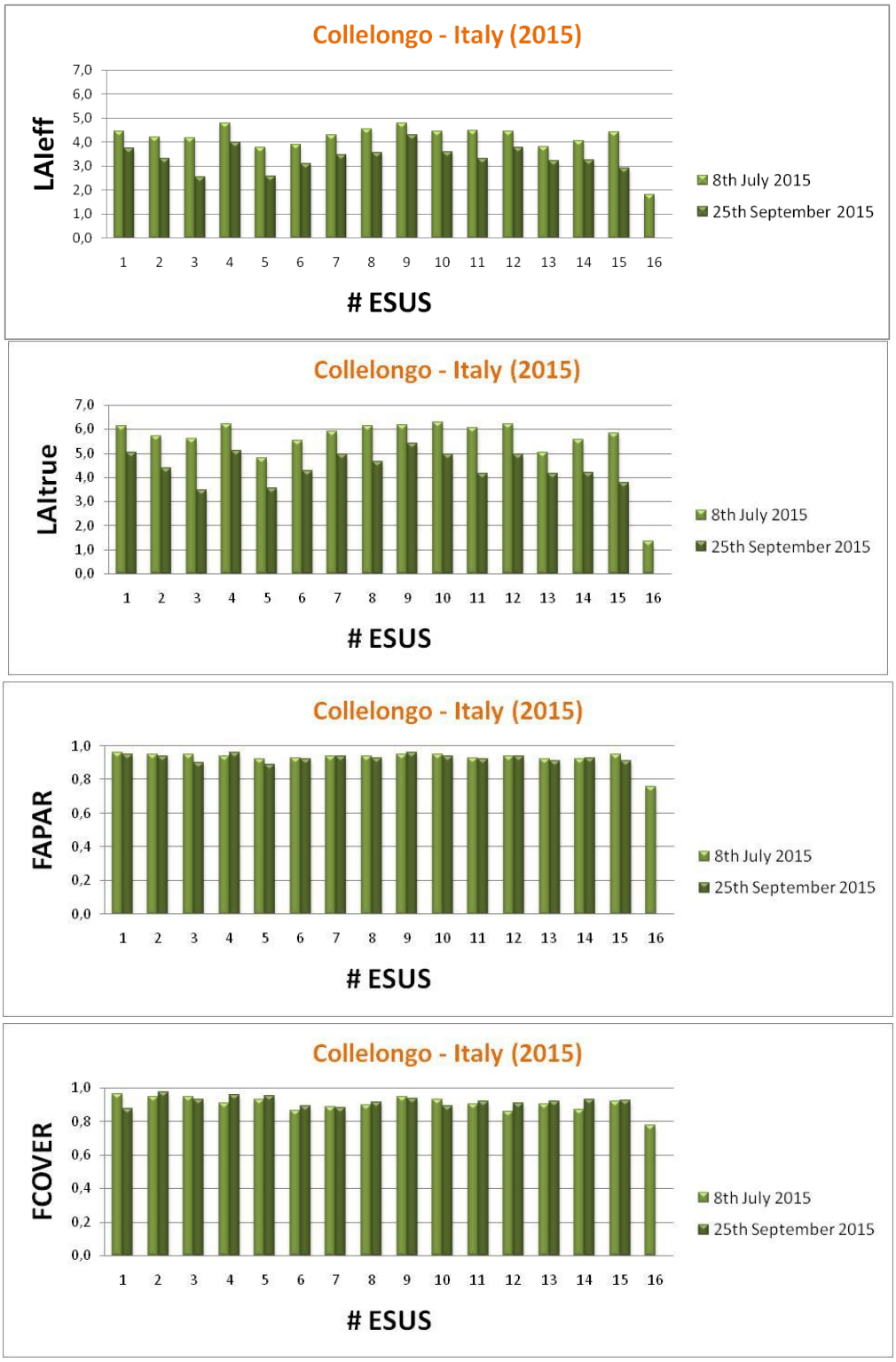

Figure 11: LAIeff, LAI, FAPAR and FCOVER measurements acquired in Collelongo site, during the field campaigns, 2015. First campaign 8th July and second campaign, 25th September.

FAPAR is very similar for all ESUs during both campaigns, ranging between 0.8 and 0.9 (Figure 11) For the FCOVER, the first campaign (8th July) shows slightly lower values, ranging typically between 0.7 and 0.8, whereas for the second campaign (25th September) the FCOVER ranges between 0.8 and 0.9. Averaged FAPAR values are 0.83 and 0.86 for the first and second campaign respectively, whereas averaged FCOVER values are 0.78 and 0.86.

The distribution of the measured variables is presented in Figure 12.

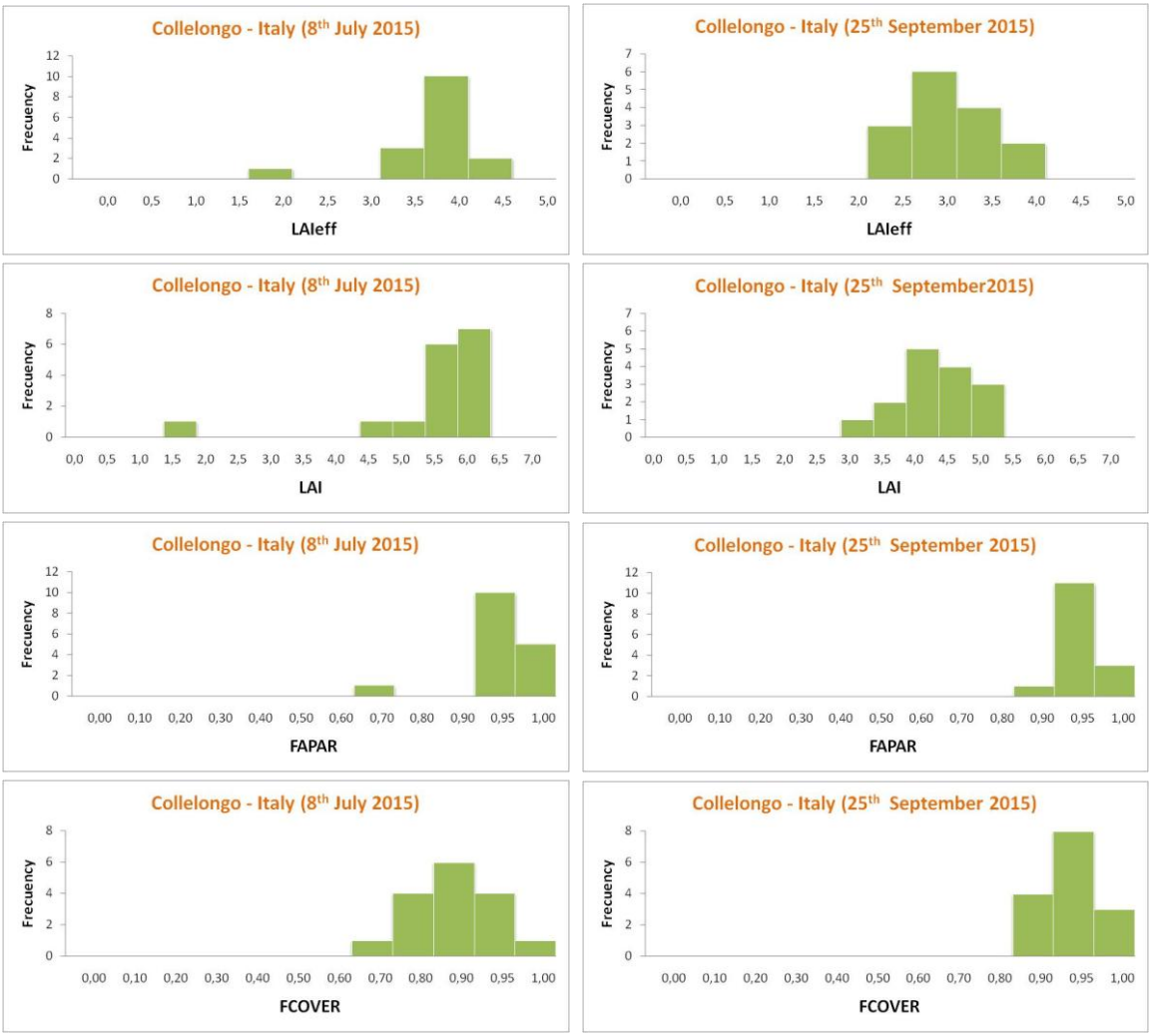

Figure 12: Distribution of the measured biophysical variables over the ESUs, Collelongo site (2015). Left: First campaign on 8th July, 2015. Right: Second campaign on 25th September, 2015.

5. EVALUATION OF THE SAMPLING

5.1. PRINCIPLES

The sampling was concentrated around the Fluxnet tower, in an area of approximately 1 km^2. The forest was very homogeneous, and the sampling was performed at the two sides of the main access road (Figure 5). The number of sampling points was only 15 due to the homogeneity of the site. The next section presents the sampling evaluation based on the convex hull.

5.2. EVALUATION BASED ON CONVEX HULL: PRODUCT QUALITY FLAG.

The interpolation capabilities of the empirical transfer function used for up-scaling the ground data using decametric images is dependent of the sampling (Martinez et al., 2009). A test based on the convex hulls was also carried out to characterize the representativeness of ESUs and the reliability of the empirical transfer function using the different combinations of the selected bands (green, red, NIR and SWIR) of the Landsat-8 image. A flag image is computed over the reflectances. The result on convex-hulls can be interpreted as:

- pixels inside the 'strict convex-hull': a convex-hull is computed using all the Landsat-8 reflectances corresponding to the ESUs belonging to the class. These pixels are well represented by the ground sampling and therefore, when applying a transfer function the degree of confidence in the results will be quite high, since the transfer function will be used as an interpolator;

- pixels inside the 'large convex-hull': a convex-hull is computed using all the reflectance combinations (±5% in relative value) corresponding to the ESUs. For these pixels, the degree of confidence in the obtained results will be quite good, since the transfer function is used as an extrapolator (but not far from interpolator);

- pixels outside the two convex-hulls: this means that for these pixels, the transfer function will behave as an extrapolator which makes the results less reliable. However, having a priori information on the site may help to evaluate the extrapolation capacities of the transfer function.

Figure 13 shows the results of the Convex-Hull test (i.e., Quality Flag image) for the Collelongo site over a 5x5 km^2 area. Despite the small number of ESUs characterized, the strict and large convex-hulls (i.e., good confidence in the transfer function) are high around the test site, 79% and 65% for the first and second field campaign respectively (Table 4). This can be explained due to the homogeneity of this site.

Table 4: Percentages of Convex hull results over the study area 5x5 km^2 in Collelongo, 2015. Convex hull values: 0= extrapolation of TF, 1= strict convex hull and 2= large convex hull.

Collelongo campaigns	Quality Flags (%)			
Field campaigns	5x5 km^2			
	0	1	2	1 & 2
8th July 2015	20	35	45	80
25th September 2015	34	18	48	66

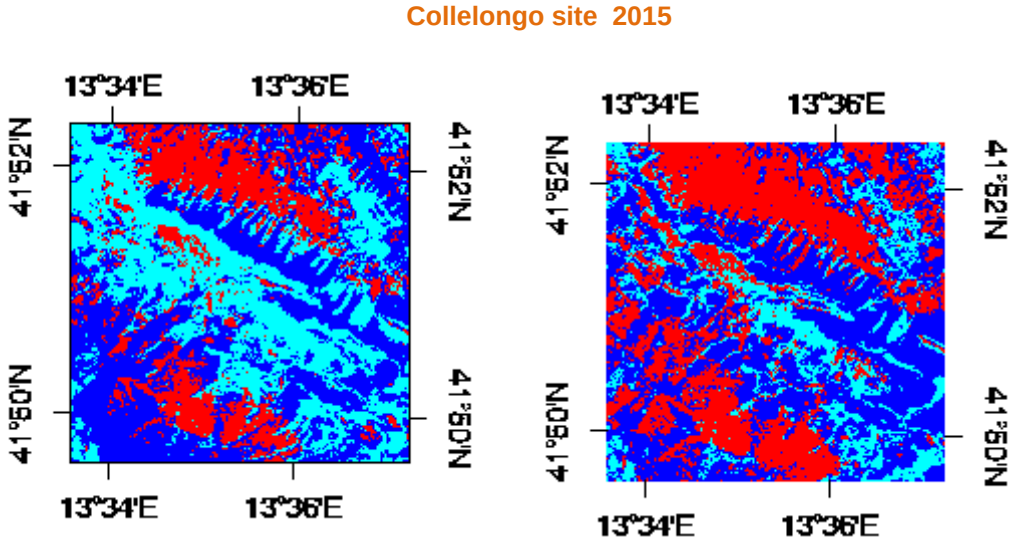

Figure 13: Convex Hull test over 5x5 km^2: clear and dark blue correspond to the pixels belonging to the 'strict' and 'large' convex hulls. Red corresponds to the pixels for which the transfer function is extrapolating, Collelongo, 2015. Left: First field campaign (8th July). Right: Second field campaign (25th September).

6. PRODUCTION OF GROUND-BASED MAPS

6.1. IMAGERY

The Landsat-8 images were acquired the 10th July and 27th August, 2015 (Table 5 for acquisition geometry). We selected 4 spectral bands from 500 nm to 1750 nm with a nadir ground sampling distance of 30 m. For the transfer function analysis, the input satellite data used is Top of Canopy (TOC) reflectance. The original projection is UTM 33 North, WGS-84

Note that for the second campaign the image acquisition is from end of August, whereas the ground data is from end of September. However, as ground measurements show a high stability from July to end of September, we assume also stability in the radiometric signal of the image.

Table 5: Acquisition geometry of Landsat-8 data used for retrieving high resolution maps.

Landsat-8 TOC METADATA		
Platform / Instrument	Landsat-8 / OLI_TIRS	
Path	190	
Row	31	
Selected Bands	B3(green) : 0.53-0.59 µm B4(red) : 0.64-0.67 µm B5(NIR) : 0.85-0.88 µm B6(SWIR1) : 1.58-1.65 µm	
	Collelongo campaigns	
	8th July, 2015	**25th September, 2015**
Acquisition date	2015.07.10 9:46:42	2015.08.27 9:46:59
Illumination Azimuth angle	131.4834º	145.269821º
Illumination Elevation angle	26.267º	36.195988º

6.2. THE TRANSFER FUNCTION

6.2.1. The regression method

If the number of ESUs is enough, multiple robust regression 'REG' between ESUs reflectance and the considered biophysical variable can be applied (Martínez et al., 2009): we used the 'robustfit' function from the Matlab statistics toolbox. It uses an iteratively re-weighted least squares algorithm, with the weights at each iteration computed by applying the bi-square function to the residuals from the previous iteration. This algorithm provides lower weight to ESUs that do not fit well.

The results are less sensitive to outliers in the data as compared with ordinary least squares regression. At the end of the processing, two errors are computed: weighted RMSE (using the weights attributed to each ESU) (RW) and cross-validation RMSE (leave-one-out method) (RC).

As the method has limited extrapolation capacities, a flag image (Figure 13), based on the convex hull test, is included in the final ground based map in order to inform the users on the reliability of the estimates.

6.2.2. Band combination

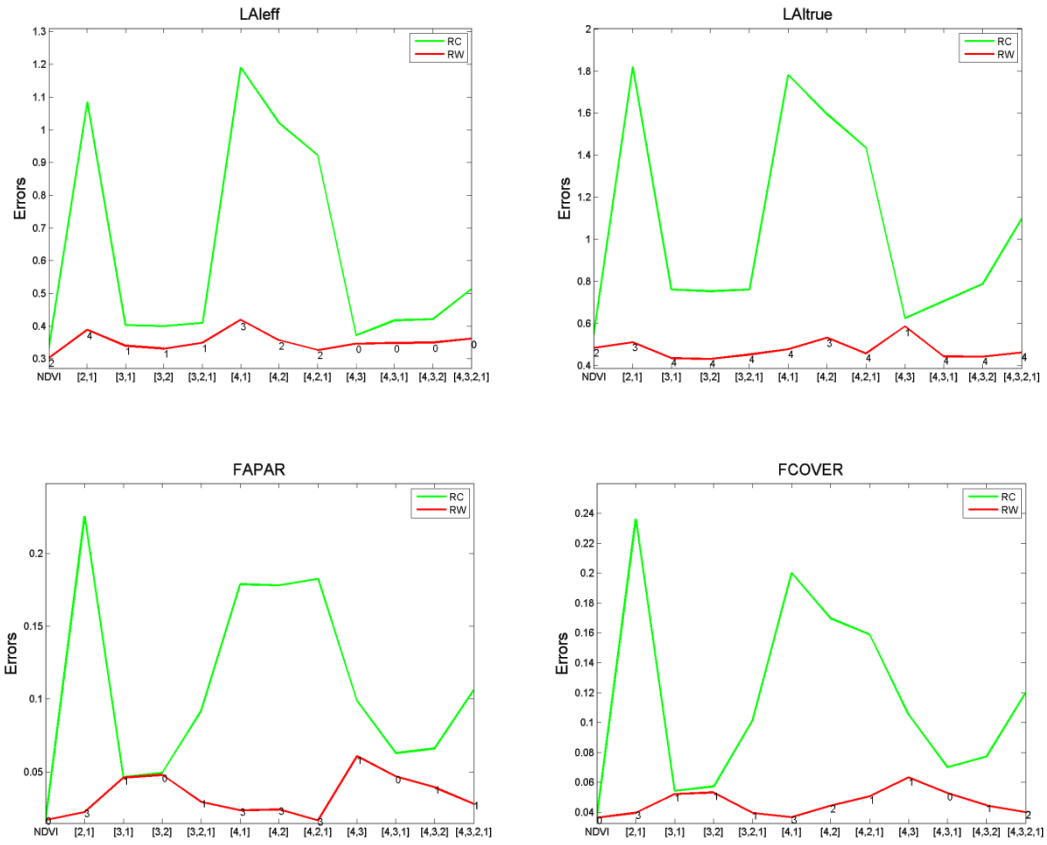

Figure 14: Test of multiple regression (TF) applied on different band combinations. Band combinations are given in abscissa (1=G, 2=RED, 3=NIR and 4=SWIR). The weighted root mean square error (RMSE) is presented in red along with the cross-validation RMSE in green. The numbers indicate the number of data used for the robust regression with a weight lower than 0.7 that could be considered as outliers. Collelongo, first field campaign on 8th July 2015.

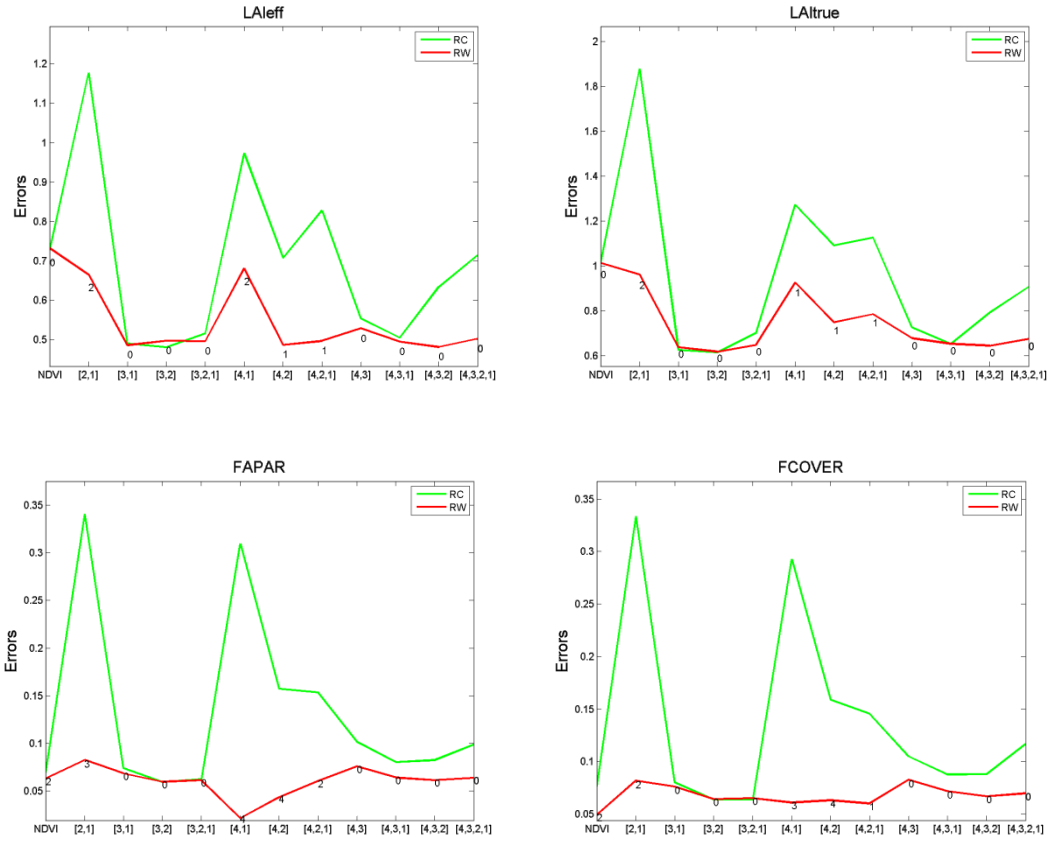

Figure 15: As in Figure 14 for the second campaign on 25th September, 2015.

Figure 14 and Figure 15 show the errors (RW, RC) obtained for the several band combinations using TOC reflectance for the first and the second campaign, respectively. We have selected the NDVI as input for the transfer function (see section 6.2.3). For the first campaign, NDVI shows lower errors than other band combinations for the FAPAR and FCOVER, whereas provides similar errors for the LAI. For the second campaign, we have selected also NDVI to keep consistency with the first campaign, and because the relationship between biophysical estimates retrieved using other band combinations shows lower consistency than using NDVI.

6.2.3. The selected Transfer Function

The applied transfer function is detailed in Table 6, along with its weighted (RW) and cross validated (RC) errors.

For the FAPAR and FCOVER, a simple linear relationship with NDVI was selected:

$$FAPAR = a + b \cdot NDVI \qquad \text{Eq. (6)}$$

$$FCOVER = a + b \cdot NDVI \qquad \text{Eq. (7)}$$

For the LAIeff and LAI, an exponential relationship with NDVI was selected according to Baret et al., (1989):

$$\mathrm{LAI} = \mathrm{a} + \mathrm{b} \cdot \ln\left(\frac{\mathrm{NDVI}_{\infty} - \mathrm{NDVI}}{\mathrm{NDVI}_{\infty} - \mathrm{NDVI}_{\mathrm{s}}}\right) \qquad \text{Eq. (8)}$$

Where b represents the extinction coefficient which depends on the average leaf angle inclination, solar zenith angle and diffuse reflectance and transmittance of the leaves. “b” was set empirically with the ground data for each transfer function, as well as the residuals “a”. NDVIs represents the typical NDVI of bare soil areas and NDVI∞ represents the NDVI of fully developed canopies, both assumed to be constant over the image. NDVIs was set to 0.18 and NDVI∞ to 0.95.

Table 6: Transfer function applied to the whole site for LAIeff, LAI, instantaneous FAPAR at 10:00 SLT and FCOVER. RW for weighted RMSE, and RC for cross-validation RMSE.

Variable	Band Combination	RW	RC
Collelongo campaign, Italy. 8th July 2015			
LAIeff	- 0.065 - 1.387· $ln\left(\frac{0.94-NDVI}{0.94-0.20}\right)$	0.30	0.32
LAI	-0.117 - 1.891 · $ln\left(\frac{0.94-NDVI}{0.94-0.20}\right)$	0.48	0.59
FAPAR	- 0.206 + 1.255·(NDVI)	0.03	0.02
FCOVER	- 0.199 + 1.22·(NDVI)	0.04	0.04
Collelongo campaign, Italy. 25th September 2015			
LAIeff	0.434 - 1.097· $ln\left(\frac{0.95-NDVI}{0.95-0.17}\right)$	0.73	0.73
LAI	0.627 - 1.425· $ln\left(\frac{0.95-NDVI}{0.95-0.17}\right)$	1.01	1.02
FAPAR	- 0.137 + 1.204·(NDVI)	0.06	0.07
FCOVER	- 0.147 + 1.194·(NDVI)	0.05	0.08

Figure 16 and Figure 17 show scatter-plots between ground observations and their corresponding transfer function (TF) estimates for the selected bands combination (i.e. the NDVI). A good correlation is observed for the LAIeff, LAI, FAPAR and FCOVER with points distributed along the 1:1 line, with no mean bias and low RMSE values, although some scattering is observed mainly for LAI.

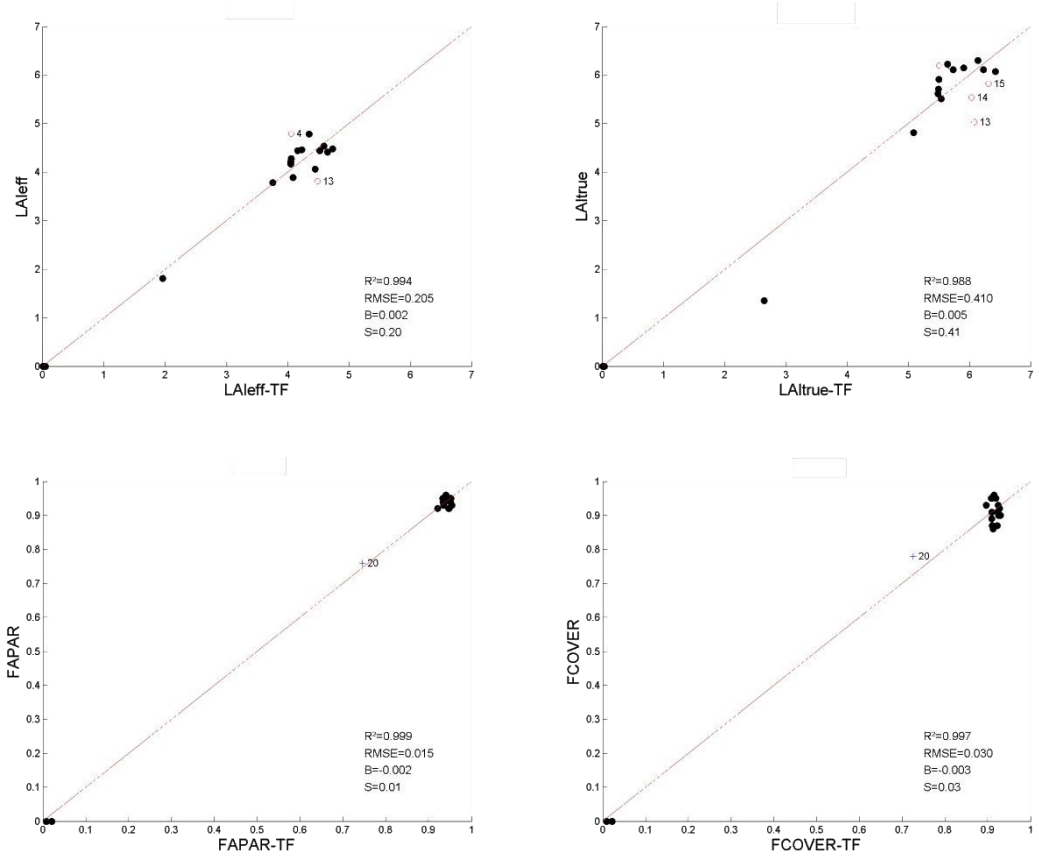

Figure 16: LAIeff, LAI, FAPAR and FCOVER results for regression on NDVI. Full dots: Weight>0.7. Empty dots: 0<Weight<0.7. Crosses: Weight=0. Collelongo site, first field campaign 2015 on 8th July, 2015.

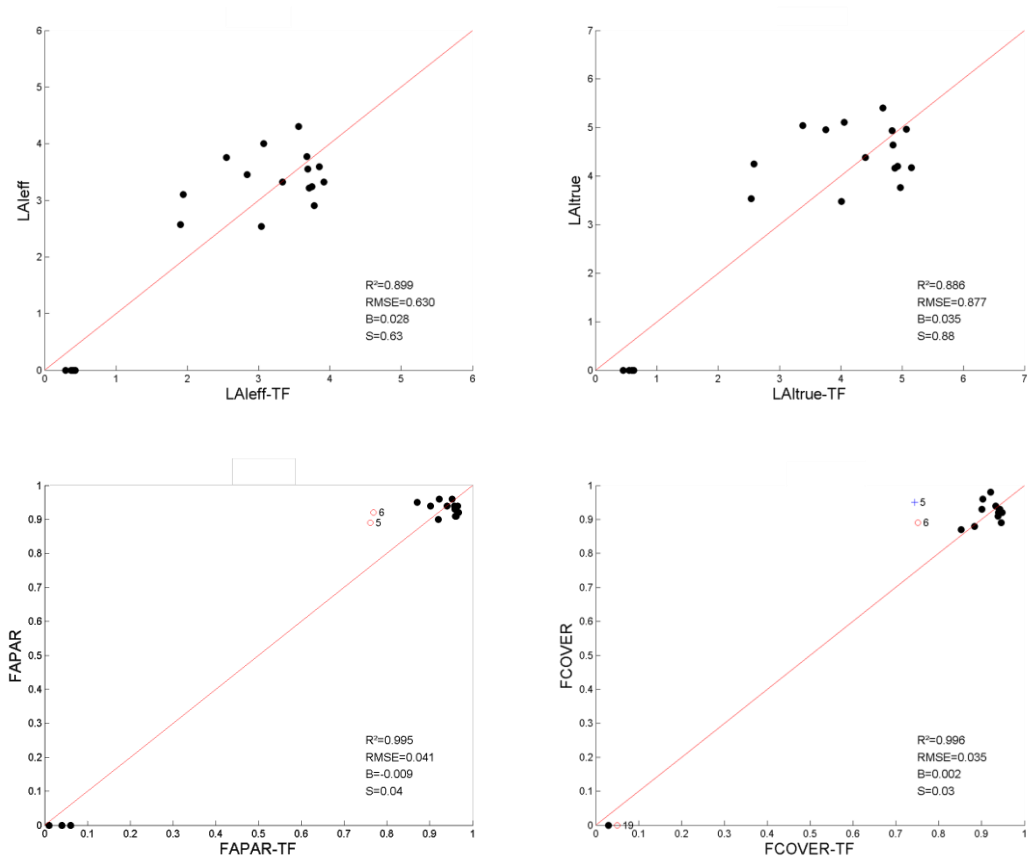

Figure 17: As in Figure 16 for the second field campaign on 25th September, 2015.

6.3. THE HIGH RESOLUTION GROUND BASED MAPS

The high resolution maps are obtained applying the selected transfer function (Table 6) to the Landsat-8 NDVI derived from TOC reflectances. The study area has been extended to 5x5km2 (centre located at 41.85º N, 13.59º E, UTM zone 33 North, Datum WGS-84). Figure 18 to Figure 21 present the ground-based maps for the several biophysical variables. Figure 13 shows the Quality Flag included in the final product.

LAIeff

8th July 2015 **25th September 2015**

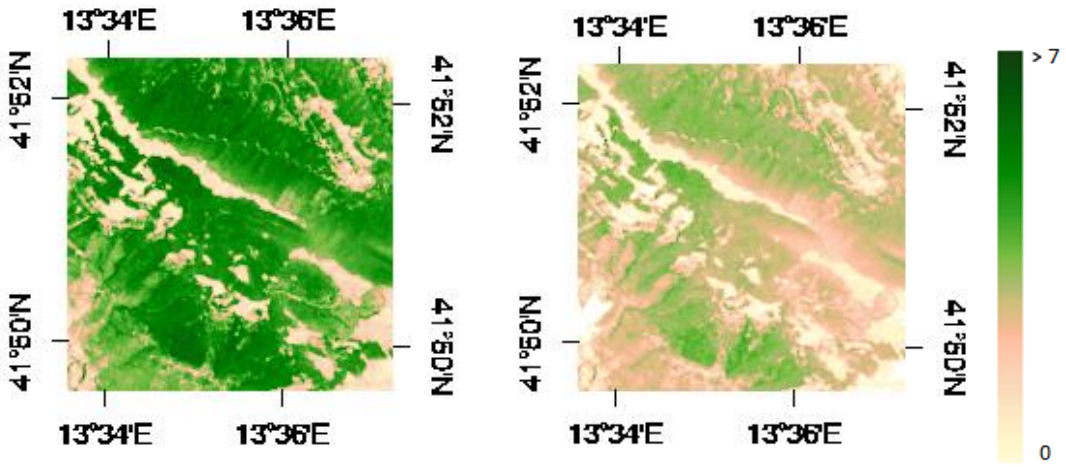

Figure 18**: Ground-based LAIeff maps (5x5 km2) over Collelongo site (Italy) 2015. Left: First field campaign (8th July). Right: Second field campaign (25th September).**

LAI

8th July 2015 **25th September 2015**

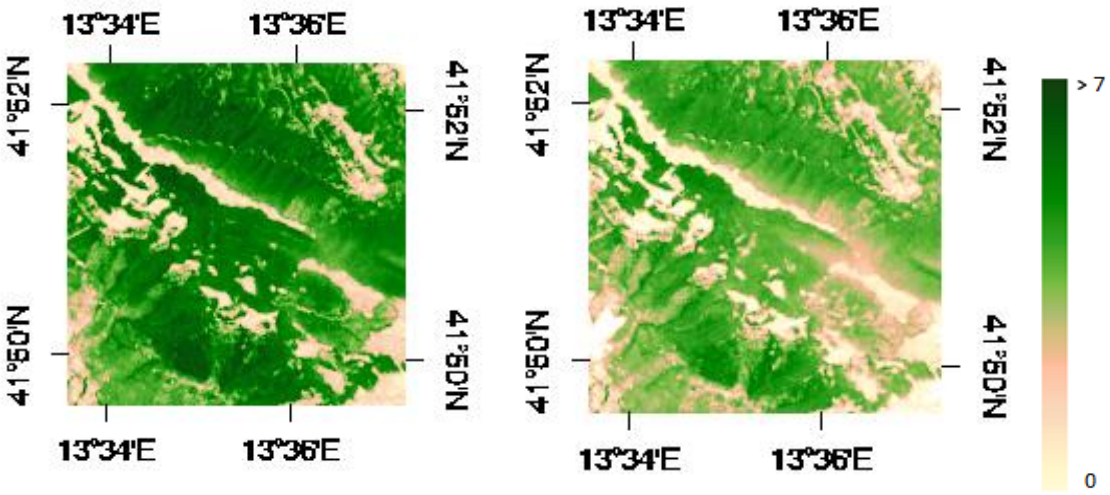

Figure 19: Ground-based LAI maps (5x5 km^2) over *Collelongo site (Italy) 2015.* Left: First field campaign (8th July). Right: Second field campaign (25th September).

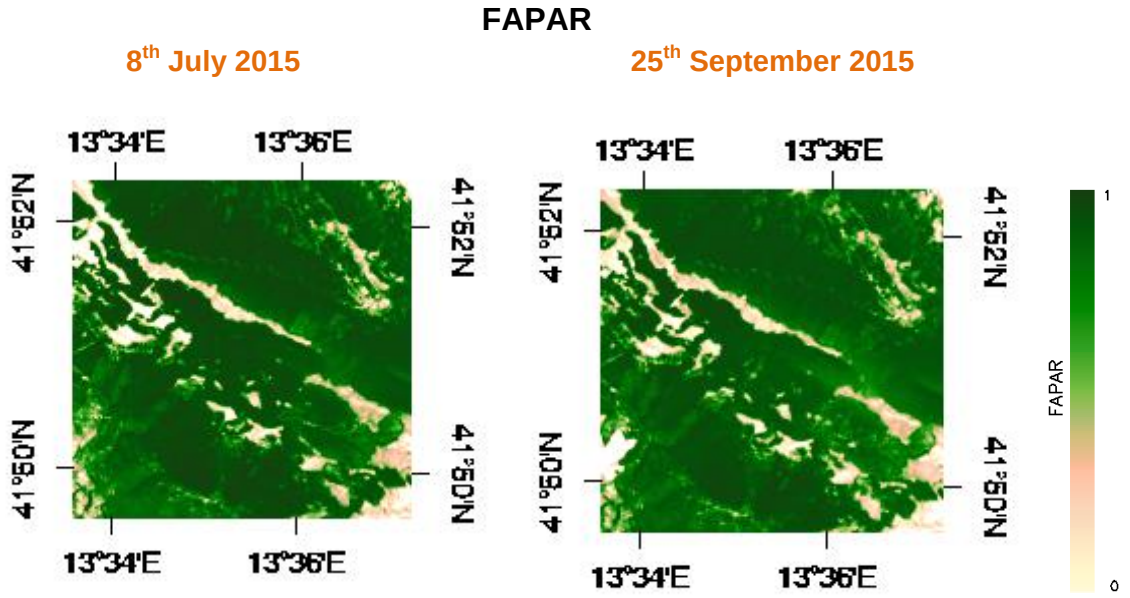

Figure 20: Ground-based maps of Instantaneous FAPAR at 10:00 SLT (5x5 km^2) over *Collelongo site* (Italy) 2015. Left: First field campaign (8th July). Right: Second field campaign (25th September).

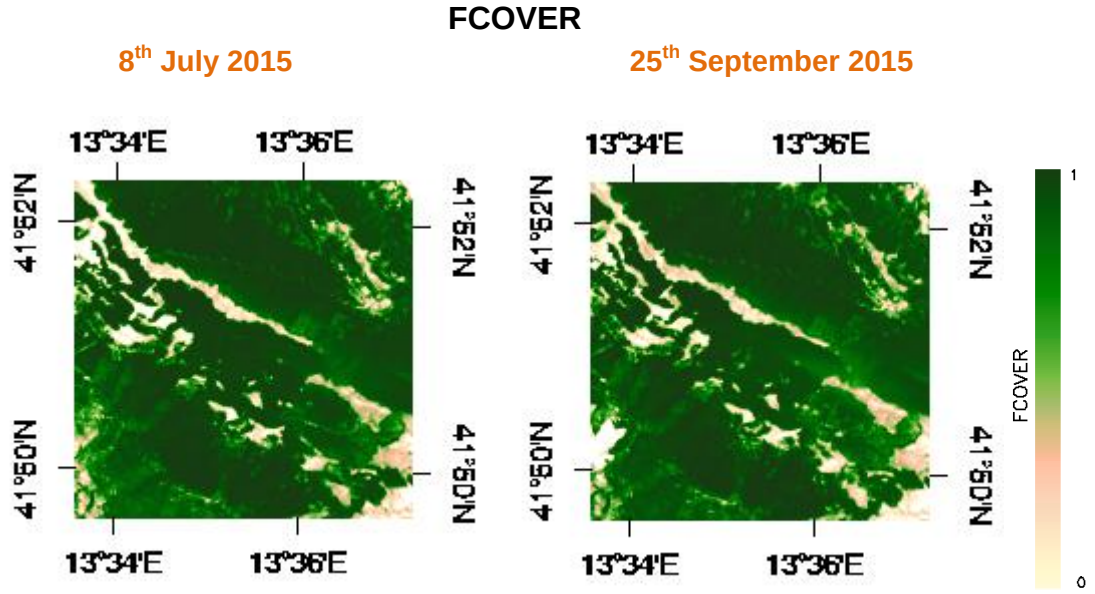

Figure 21: Ground-based FCOVER map (5x5 km^2) over *Collelongo site (Italy) 2015.* Left: First field campaign (8th July). Right: Second field campaign (25th September).

Figure 22 shows several scatters plots between biophysical variables that prove the good consistency of the ground-based maps, showing the exponential (LAI vs FAPAR) and linear (FAPAR vs FCOVER) trend observed with the ground data.

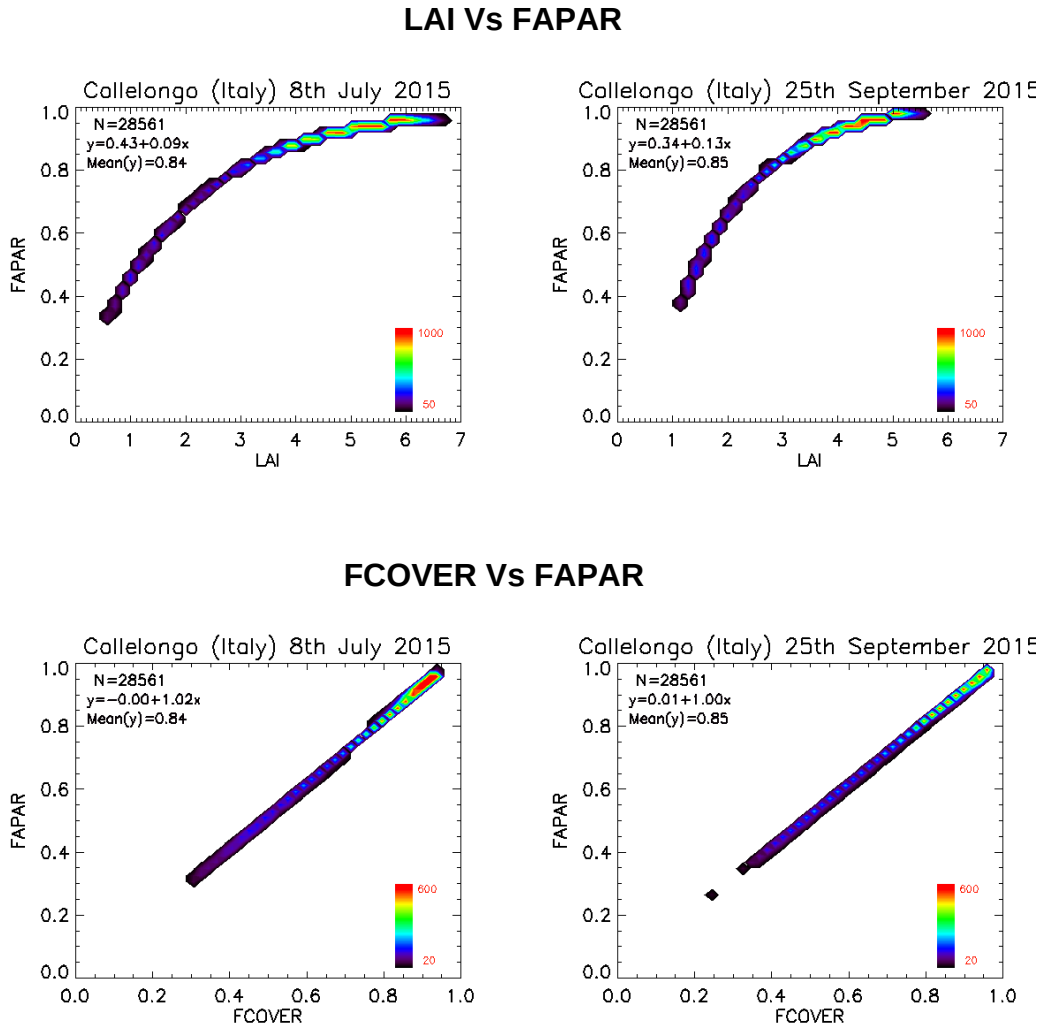

Figure 22: Scatter plots LAI vs FAPAR and FAPAR vs FCOVER for the two campaigns over *Collelongo site (Italy) 2015.* Left: First field campaign (8th July). Right: Second field campaign (25th September).

6.3.1. Mean Values

Mean values of a 3x3 km2 area centred in the test site are provided for the validation of 1 km satellite products in agreement with the CEOS OLIVE direct dataset (Table 7). For the validation of coarser resolutions product (e.g. MSG products) a larger area should be considered. Mean values are slightly lower than the average of the ground measurements, due to the impact of areas with low vegetation.

Table 7: Mean values and standard deviation (STD) of the HR biophysical maps for the selected 3 x 3 km^2 areas at Collelongo site (Italy) 2015.

3x3 km^2	Collelongo campaign							
	Mean Values				STDV Values			
	LAIeff	LAI	FAPAR	FCOVER	LAIeff	LAI	FAPAR	FCOVER
8th July 2015	3,38	4,58	0,87	0,84	1,06	1,44	0,13	0,13
25th September 2015	2,92	3,86	0,87	0,86	0,79	1,02	0,13	0,13

Table 8 describes the content of the geo-biophysical maps in the "BIO_YYYYMMDD_LANDSAT8_ Collelongo_ETF_5x5" files.

Nomenclature: BIO_YYYYMMDD_SENSOR_Site_ETF_Area
where:

BIO stands for Biophysical (LAIeff, LAI, FAPAR and FCOVER)

SENSOR = LANDSAT8

YYYYMMDD = Campaign date

Site = Collelongo

ETF stands for Empirical Transfer Function

Area = window size 5x5

Table 8: Content of the dataset.

Parameter	Dataset name	Range	Variable Type	Scale Factor	No Value
LAI effective	LAIeff	[0, 7]	Integer	1000	-1
LAI	LAI	[0, 7]	Integer	1000	-1
FAPAR 10:00 SLT	FAPAR	[0, 1]	Integer	10000	-1
Fraction of Vegetation Cover	FCOVER	[0, 1]	Integer	10000	-1
Quality Flag	QFlag	0,1,2 (*)	Integer	N/A	-1

(*) 0 means extrapolated value (low confidence), 1 strict interpolator (best confidence), 2 large interpolator (medium confidence).

7. CONCLUSIONS

The FP7 ImagineS project continues the innovation and development activities to support the operations of the Copernicus Global Land service. One of the sites characterized in the framework of the ImagineS project is the Collelongo-Selvapiana beech forest site, in Italy. The permanent experimental site was installed in 1991 by the Department of Forest Environment and Resources, University of Tuscia, Viterbo and take part in several international networks as CarboEurope, FluxNet or ICP-Forests.

This report firstly presents the ground data collected during two field campaigns on 8th of July and 25th of September, 2015 by EOLAB and IBAF, respectively. The dataset includes 15 elementary sampling units where digital hemispherical photographs, were taken and processed with the CAN-EYE software to provide LAI, LAIeff, FAPAR and FCOVER values.

Secondly, high resolution ground-based maps of the biophysical variables have been produced over the site using Landsat-8 TOC reflectance data, according to the CEOS LPV recommendations for validation of low resolution satellite sensors. Transfer functions have been derived by multiple robust regressions between ESUs reflectance and the several biophysical variables. NDVI has been selected as input for the transfer function (exponential relationship with LAIeff and LAI, and linear relationship with FAPAR and FCOVER). NDVI assures good consistency of the maps over the whole area. The RMSE values for the several transfer function estimates are 0.21 and 0.63 for LAIeff, 0.41 and 0.87 for LAI, 0.02 and 0.04 for instantaneous FAPAR at 10:00 SLT and, finally, 0.03 and 0.04 for FCOVER, for the two field campaigns respectively.

The quality flag map based on the convex-hull analysis shows good confidence in 80% for the first campaign and 66% for the second.

The biophysical variable maps are available in geographic (UTM 33 North projection WGS-84) coordinates at 30 m resolution. Mean values and standard deviation for LAIeff, LAI, FCOVER and FAPAR were computed over an area of 3x3 km^2 for validation of low and medium resolution satellite products.

8. ACKNOWLEDGEMENTS

This work is supported by the FP7 IMAGINES project under Grant Agreement N°311766. Landsat-8 HR imagery is provided through the USGS Global Visualization service. This work is done in collaboration with the consortium implementing the Global Component of the Copernicus Land Service.

Thanks to the IBAF (Institute of Agro-Environmental & Forest Biology of the National Research Council - CNR) for providing ground datasets and the support and the organization of the field campaigns, and the facilities which allow us to properly characterize the site.

9. REFERENCES

Baret, F., de Solan, B., Lopez-Lozano, R., Ma, K. and Weiss, M. (2010) GAI estimates of row crops from downward looking digital photos taken perpendicular to rows at 57.5º zenith angle: theoretical considerations based on 3D architecture models and application to wheat crops. Agricultural and Forest Metereology. 150, 1393-1401.

Baret, F and Fernandes, R. (2012). Validation Concept. VALSE2-PR-014-INRA, 42 pp.

Berguer. M. M. Rast, P. Wursteisen, E. Attema, J. Moreno, et al. (2001). The DAISEX campaigns in support of a future land-surface-processes mission. Esa bulletin, Bulletin ASE. European Space Agency, nº105: 101-111, February 2001.

Camacho, F., Cernicharo, J., Lacaze, R., Baret, F., and Weiss, M. (2013). GEOV1: LAI, FAPAR Essential Climate Variables and FCOVER global time series capitalizing over existing products. Part 2: Validation and intercomparison with reference products. *Remote Sensing of Environment, 137: 310-329.*

Chiti T, Papale D, Smith P, Dalmonech D, Matteucci G, Yeluripati J, Rodeghiero M, Valentini R (2010) Predicting changes in soil organic carbon in mediterranean and alpine forests during the Kyoto Protocol commitment periods using the CENTURY model. Soil Use Manage 26:475–484.

Demarez, V., Duthoit, S., Baret, F., Weiss, M. and Dedieu, G. (2008). Estimation of leaf area and clumping indexes of crops with hemispherical photographs. *Agricultural and Forest Meteorology. I48, 644-655*.

Fernandes, R., Plummer, S., Nightingale, J., et al. (2014). Global Leaf Area Index Product Validation Good Practices. CEOS Working Group on Calibration and Validation - Land Product Validation Sub-Group. *Version 2.0: Public version made available on LPV website*.

Guidolotti, G., Rey, A., D'andrea, E., Matteucci, G., De Angelis, P., 2013. Effect of environmental variables and stand structure on ecosystem respiration components in a Mediterranean beech forest. Tree Physiol. 33, 960–972. doi:10.1093/treephys/tpt065

Latorre, C., Camacho, F., Pérez, M., Beget M.E. and Di Bella, C. (2014). "Vegetation Field Data and Production of Ground-Based Maps: 25 de Mayo site. La Pampa, Argentina" report. 18 -20 (Available at ImagineS website: http://fp7-imagines.eu/pages/documents.php).

Martínez, B., García-Haro, F. J., & Camacho, F. (2009). Derivation of high-resolution leaf area index maps in support of validation activities: Application to the cropland Barrax site. *Agricultural and Forest Meteorology, 149, 130–145*.

Matteucci G, Masci A, Valentini R, Scarascia G (2007) The response of forests to global change: measurements and modelling simulations in a mountain forest of the Mediterranean Region. In: Palahi M, Byrot Y, Rois M (eds) Scientific tools and research needs for multifunc-

tional Mediterranean forest ecosystem management. Vol. 56. EFI Proceedings, Joensuu, Finland, pp 11–23. ISBN 978-952-5453-18- 8, ISBN 978-952-5453-19-5 (on line).

Miller, J.B. (1967). A formula for average foliage density. Aust. J. Bot., 15:141-144

Morisette, J. T., Baret, F., Privette, J. L., Myneni, R. B., Nickeson, J. E., Garrigues, S., et al. (2006). Validation of global moderate-resolution LAI products: A framework proposed within the CEOS land product validation subgroup. *IEEE Transactions on Geoscience and Remote Sensing, 44, 1804–1817*.

Scartazza, A., Moscatello, S., Matteucci, G., Battistelli, A., Brugnoli, E., 2013. Seasonal and inter-annual dynamics of growth, non-structural carbohydrates and C stable isotopes in a Mediterranean beech forest. Tree Physiol. 33, 730–742. doi:10.1093/treephys/tpt045

Valentini R, De Angelis P, Matteucci G, Monaco R, Dore S, Scarascia Mugnozza G (1996) Seasonal net carbon dioxide exchange of a beech forest with the atmosphere. Global Change Biol 2:199–207.

Weiss, M., Baret, F., Smith, G.J., Jonckheere, I. and Coppin, P., (2004). Review of methods for in situ leaf area index (LAI) determination. Part II. Estimation of LAI, errors and sampling. *Agricultural and Forest Meteorology. 121, 37–53*.

Weiss M. and Baret F. (2010). CAN-EYE V6.1 User Manual

Welles, J.M. and Norman, J.M., 1991. Instrument for indirect measurement of canopy architecture. Agronomy J., 83(5): 818-825.